# Estimation of the Antarctic surface mass balance using MAR (1979-2015) and identification of dominant processes

Cécile Agosta[1,2,3], Charles Amory[1], Christoph Kittel[1], Anais Orsi[2], Vincent Favier[3], Hubert Gallée[3], Michiel R. van den Broeke[4], Jan T. M. Lenaerts[4,5], Jan Melchior van Wessem[4], Willem Jan van de Berg[4], and Xavier Fettweis[1]

[1]F.R.S.-FNRS, Laboratory of Climatology, Department of Geography, University of Liège, B-4000 Liège, Belgium
[2]Laboratoire des Sciences du Climat et de l'Environnement (IPSL/CEA-CNRS-UVSQ UMR 8212), CEA Saclay, F-91190 Gif-sur-Yvette, France
[3]Université Grenoble Alpes, CNRS, Institut des Géosciences de l'Environnement, F-38000, Grenoble,France
[4]Institute for Marine and Atmospheric Research Utrecht, Utrecht University, Utrecht, the Netherlands
[5]Department of Atmospheric and Oceanic Sciences, University of Colorado Boulder, Boulder CO, United States of America

**Correspondence:** Cécile Agosta (cecile.agosta@gmail.com)

**Abstract.** The Antarctic ice sheet mass balance is a major component of the sea level budget and results from the difference of two fluxes of a similar magnitude: ice flow discharging in the ocean and net snow accumulation on the ice sheet surface, i.e. the surface mass balance (SMB). Separately modelling ice dynamics and surface mass balance is the only way to project future trends. In addition, mass balance studies frequently use regional climate models (RCMs) outputs as an alternative to observed fields because SMB observations are particularly scarce on the ice sheet. Here we evaluate new simulations of the polar RCM MAR forced by three reanalyses, ERA-Interim, JRA-55 and MERRA2, for the period 1979-2015, and we compare ~~our~~ MAR results to the last outputs of the RCM RACMO2 forced by ERA-Interim. We show that MAR and RACMO2 perform similarly well in simulating coast to plateau SMB gradients, and we find no significant differences in their simulated SMB when integrated over the ice sheet or its major basins. More importantly, we outline and quantify missing processes in both RCMs. Along stake transects, we show that both models accumulate too much snow on crests, and not enough snow in valleys, as a result of ~~erosion-deposition processes~~ drifting snow transport fluxes not included in MAR ~~, where the drifting snow module has been switched off,~~ and probably underestimated in RACMO2 by a factor of three. ~~As a consequence, the amount of drifting snow sublimating in the atmospheric boundary layer remains a potentially large mass sink needed~~ Our results tend to confirm that drifting snow transport and sublimation fluxes are much larger than previous model-based estimates and need to be better ~~constrained. Moreover,~~ resolved and constrained in climate models. MAR generally simulates larger SMB and snowfall amounts than RACMO2 inland, ~~whereas snowfall rates are significantly lower in MAR than in RACMO2~~ particularly on the lee side of topographic barriers, whereas lower snowfall amount are found windward of topographic barriers and in valleys at the ice sheet margins. ~~This divergent behaviour at the margins results from differences in model parameterisations, as MAR explicitly advects precipitating particles through the atmospheric layers and sublimates snowflakes in the undersaturated katabatic layer, whereas in RACMO2 precipitation is added to the surface without advection through the atmosphere. Consequently, we corroborate a recent study concluding that sublimation of precipitation~~ The amount of precipitation lost by sublimation in the low-level atmospheric layers ~~is a significant mass sink for the Antarctic SMB, as~~

it may represent ~~~240±25~~ in MAR represents 363 Gt yr$^{-1}$ ~~of difference in snowfall between RACMO2 and MAR for the period 1979-2015~~over the grounded ice sheet for the year 2015, which is ~~10~~16% of the simulated snowfall ~~loaded on the ice sheet and~~ load at the ground. This estimate is consistent with a recent study based on precipitation radar observations, and is more than twice ~~the surface snow sublimation as currently simulated by MAR.~~ as much as simulated by RACMO2, because of different time residence of precipitating particles in the atmosphere. Atmospheric sublimation is largely responsible for the much lower snowfall rates in MAR than in RACMO2 in katabatic channels at the ice sheet margins. The remaining spatial differences in snowfall between MAR and RACMO2 are attributed to differences in advection of precipitation inland, which is probably overestimated in MAR.

## 1 Introduction

Mass loss from the Antarctic ice sheet (AIS) and therewith its contribution to the sea level budget results from the difference of two fluxes of a similar magnitude: ice flow discharging in the ocean (D) and net snow accumulation on the ice sheet surface, i.e. the surface mass balance (SMB). The total ice sheet mass balance (SMB minus D) can be assessed using ~~several approaches (Shepherd et al., 2012), but~~ satellite altimetry, gravimetry or the input–output method (Shepherd et al., 2018), which all request surface mass balance estimates. The input-output method, which consists in separately modelling ice dynamics and surface mass balance, ~~called the input-output method, is~~ is also the only way to project future trends.

Surface mass balance as used in this study is the sum of mass gains (mainly snowfall accumulation and some riming), mass losses (mainly surface and drifting snow sublimation, some liquid water runoff) and ~~redistribution of snow by the wind,~~ drifting snow transport (defined as the horizontal advection of the drifting snow) which can lead to either ~~deposition (mass gain ) or erosion (mass loss)~~mass gain or mass loss. Snowfall rates are one order of magnitude larger than all of the other SMB fluxes at the continental scale (Lenaerts et al., 2012b), with the largest amounts found along the ice sheet margins due to cyclonic activity in the Southern Ocean and to the orographic lifting of relatively warm and moist air masses (van Wessem et al., 2014; Favier et al., 2017). Accumulation patterns are highly variable at the kilometre scale and from year to year (e.g., Agosta et al., 2012). Consequently, proper observations of SMB require a high spatial coverage (e.g. stake-lines, accumulation radars plus ice-cores for layer dating and snow density) and a temporal sampling spanning several years (Eisen et al., 2008). Even if efforts have been made to fulfil those requirements, ground-based observations are scarce and carry with them high logistical costs in this cold, windy and remote environment. Interpolation techniques used to interpolate the scarce SMB observations (Vaughan et al., 1999; Arthern et al., 2006) encounter major caveats (Magand et al., 2008; Genthon et al., 2009; Picard et al., 2009).

This is why many AIS mass balance studies use output of regional climate models (RCMs) to estimate ice sheet SMB for the recent decades ~~(e.g., Rignot et al., 2011; Shepherd et al., 2012; Gardner et al., 2018)~~(e.g., Rignot et al., 2011; Gardner et al., 2018; Shephe . In order to obtain a good agreement with observations, atmospheric models require accurate large-scale circulation patterns together with a proper representation of snow surface processes, clouds, turbulent fluxes, and a relatively high horizontal resolution to properly resolve the complex ice sheet topography at the margins.

Here, we ~~compare SMB fields of the state-of-the-art regional climate model RACMO2 (van Wessem et al., 2017) with~~ present new simulations of the regional climate model MAR, applied ~~here~~ for the first time over the whole AIS, but already widely used for polar studies, e.g. in Greenland (Fettweis et al., 2013, 2017), Svalbard (Lang et al., 2015), Adélie Land (Antarctic coastal area, Gallée et al., 2013; Amory et al., 2015) and Dome C (Antarctic plateau, Gallée et al., 2015). We compare MAR-simulated SMB with the state-of-the-art regional climate model RACMO2 (van Wessem et al., 2018). We use available SMB observational datasets to show that ~~both~~ MAR and RACMO2 perform similarly well in simulating the SMB ~~fields~~spatial gradients. In addition, we identify significant processes that still need to be included ~~and~~/or improved in both RCMs.

In Section 2, we describe MAR and its specific set-up for Antarctica, together with RACMO2, the forcing fields, observational datasets and methods designed for model evaluation. In Section 3, we show that both RCMs share common biases against observed SMB, resulting from ~~erosion-deposition processes~~drifting snow transport fluxes. Secondly, we analyse SMB differences between models and show that many of the discrepancies can be attributed to low-level sublimation of precipitation in katabatic channels and to the difference in precipitation advection inland. Finally, in Section 4, we summarise our main findings and discuss further efforts to be achieved for a better assessment of the AIS surface mass balance.

## 2 Data and methods

### 2.1 Regional modelling

#### 2.1.1 Regional atmospheric models

For the first time, the polar-oriented regional atmospheric model MAR is applied for decades-long simulations over the whole Antarctic ice sheet. MAR atmospheric dynamics are based on the hydrostatic approximation of the primitive equations, fully described in Gallée and Schayes (1994). Prognostic equations are used to depict five water species: specific humidity, cloud droplets and ice crystals, raindrops and snow particles (Gallée, 1995). Sublimation of airborne snow particles is a direct contribution to the heat and moisture budget of the atmospheric layer in which these particles are simulated. The radiative transfer through the atmosphere is parametrised as in Morcrette (2002), with snow particles affecting the atmospheric optical depth (Gallée and Gorodetskaya, 2010). The atmospheric component is coupled to the surface scheme SISVAT (soil ice snow vegetation atmosphere transfer, De Ridder and Gallée, 1998) dealing with the energy and mass exchanges between surface, snow and atmosphere. The snow–ice part of SISVAT is based on the snow model CROCUS (Brun et al., 1992). It is a one-dimensional multilayered energy balance model which simulates meltwater refreezing, snow metamorphism and snow surface albedo depending on snow properties. We used MAR version 3.6.4, simply called MAR here-after. In this version the physical settings are the same as in MAR version 3.5.2 used for Greenland (Fettweis et al., 2017), except for the adaptations detailed below.

*Grid:* Projection is the standard Antarctic polar stereographic (EPSG:3031). The horizontal resolution is 35 km, an intermediate resolution that results from a computation time compromise in order to run the model with multiple reanalyses and global climate model forcings over the 20th and the 21st century. The vertical discretisation is composed of 23 hybrid levels from $\sim$2 m to $\sim$17000 m above the ground.

*Boundaries:* The topography is derived from the Bedmap2 surface elevation dataset (Fretwell et al., 2013). Because the Antarctic domain is about 4 times larger than the Greenland domain, the circulation has to be more strongly constrained. This is why we use a boundary relaxation of temperature and wind in the upper atmosphere starting from 400 hPa ($\sim$6000 m above the ground) to 50 hPa (upper level), as in van de Berg and Medley (2016), whereas relaxation starts from 200 hPa in Fettweis et al. (2017).

*Parameterisations:*

a) The ~~fresh~~ surface snow density $\rho_s$ is computed as a function of 10 m wind speed $ws_{10}$ (m s$^{-1}$) and surface temperature $T_s$ (K):

$$\rho_s = 149.2 + 6.84\,ws_{10} + 0.48\,T_s, \tag{1}$$

with minimum-maximum values of 200–400 kg m$^{-3}$. This parameterisation was defined so that the simulated density of the first 50 cm of snow fits observations collected over the Antarctic ice sheet (see Fig. S1, with snow density database detailed in Table S1).

b) The aerodynamic roughness length $z_0$ is computed as a function of the air temperature, as proposed in Amory et al. (2017). The parameterisation was tuned so that $z_0$ fit the observed seasonal variation between high (> 1 mm) summer and lower (0.1 mm) winter values in coastal Adélie Land, for air temperatures above -20 °C. For lower temperatures, $z_0$ is kept constant and set to 0.2 mm, in agreement with observed $z_0$ values on the Antarctic Plateau (e.g., Vignon et al., 2016);

c) As in Fettweis et al. (2017), ~~drifting snow~~ the MAR drifting snow scheme is not activated~~. Amory et al. (2015) shown that the drifting snow routine~~, because this scheme was sensitive to parameter choices ~~. Given that an~~ (Amory et al., 2015). An updated version of ~~this routine is under evaluation against satellite and ground-based observations over the whole Antarctic ice sheet, we decided to switch off the drifting snow for our first Antarctic-scale MAR simulations~~the drifting snow scheme is currently being developed and evaluated for application at the scale of the whole ice sheet.

We compare ~~the~~ MAR results over the AIS to the latest outputs of the regional atmospheric model RACMO2 version 2.3p2 ~~(van Wessem et al., 2017)~~(van Wessem et al., 2018), called RACMO2 here-after, using a horizontal resolution of 27 km and a vertical resolution of 40 atmospheric levels. This regional model is developed by the Royal Netherlands Meteorological Institute (KNMI), and has subsequently been adapted for modelling the Antarctic climate and its surface mass balance (van de Berg et al., 2006). It includes a ~~snowdrift~~ drifting snow scheme (Lenaerts et al., 2012a), an albedo routine with prognostic snow grain size (Kuipers Munneke et al., 2011), and a multilayer snow model computing melt, percolation, refreezing and runoff (Ettema et al., 2010).

MAR and RACMO2 models were developed independently. We will not detail here the many physical parameterisation differences between both RCMs, but we will later highlight some of them we show having a significant impact on the modelled SMB.

### 2.1.2 Forcing reanalyses

Regional atmospheric models are forced by atmospheric fields at their lateral boundaries (pressure, wind, temperature, humidity), at the top of the troposphere (temperature, wind), as well as by sea surface conditions (sea ice concentration, sea surface temperature) every six hours. Consequently, regional atmospheric models add details and physics to the forcing model in the mid and lower troposphere and at the land or iced surface, whereas large-scale circulation patterns are driven by the forcing fields. We forced MAR with three reanalyses over Antarctica in order to evaluate the uncertainty in the simulated surface climate arising from the uncertainty in the assimilation systems: the European Centre for Medium-Range Weather Forecasts "Interim" re-analysis (here-after ERA-Interim, resolution $\sim$0.75°, i.e. $\sim$50 km at 70 °S, Dee et al., 2011), the Modern-Era Retrospective analysis for Research and Applications Version 2 (here-after MERRA2, resolution $\sim$0.5°, Gelaro et al., 2017), and the Japanese 55-year Reanalysis from the Japan Meteorological Agency (here-after JRA-55, resolution $\sim$1.25°, Kobayashi et al., 2015).

The regional atmospheric model RACMO2 is forced by ERA-Interim. We focus our study to the period 1979-2015, as reanalyses are known to be unreliable before 1979, when satellite sounding data started to be assimilated (Bromwich et al., 2007).

### 2.2 Observations

#### 2.2.1 SMB observations and sectors of strong SMB gradients

We use surface mass balance observations of the GLACIOCLIM-SAMBA dataset detailed in Favier et al. (2013) and updated by Wang et al. (2016). This dataset is an update of the one assembled by Vaughan et al. (1999) following the quality-control methodology defined by Magand et al. (2007). It includes 3043 reliable SMB values averaged over more than 3 years. We add accumulation estimates from Medley et al. (2014), retrieved over the Amundsen Sea coast (Marie Byrd Land) with an airborne-radar method combined with ice-core glaciochemical analysis.

The first order feature of the Antarctic SMB is a strong coastal-inland gradient, with mean values ranging from typically greater than 500 $\mathrm{kg\ m^{-2}\ yr^{-1}}$ at the ice sheet margins to about 30 $\mathrm{kg\ m^{-2}\ yr^{-1}}$ in the dry interior plateau (Fig. 1, see also, e.g., Wang et al., 2016). We divide the sparse observation dataset (Fig. 1 – 5% of MAR grid cells coverage of the ice sheet) into 10 sectors detailed in Table 1 and shown in Fig. 2. Six of them are stake transects with a stake every $\sim$1.5 km, which have been proven very valuable for evaluating modelled SMB (Agosta et al., 2012; Favier et al., 2013; Wang et al., 2016). The four other sectors are composed of more scattered observations covering large elevation ranges (Victoria Land, Dronning Maud Land, and Ross Ice Shelf–Mary Byrd Land).

#### 2.2.2 Model-observation comparison method

RACMO2 outputs are bi-linearly interpolated to the $35\times35$ km MAR grid. For each SMB observation, we consider the 4 surrounding MAR grid cells, from which we eliminate ocean grid cells. We also eliminate surrounding grid cells with an

**Table 1.** Sectors extracted from the GLACIOCLIM-SAMBA database.

| Sector name | Sector type | Nb. of obs. | Nb. of grid cells | Year range | Elevation range (m) | Ref. |
|---|---|---|---|---|---|---|
| Marie Byrd Land | Radar transects | 6615 | 57 | 1980–2009 | 973–1873 | [1] |
| Ross–Mary Byrd Land | Scattered | 72 | 51 | 1950–1991 | 37–1995 | [2,3,4] |
| Victoria Land | Scattered | 60 | 40 | 1951–2006 | 1804–3240 | [5,6,7] |
| Dumont-d'Urville–Dome C | Transect | 116 | 24 | 1955–2010 | 633–3240 | [5,8,9,10] |
| Law Dome–Wilkes Land | Transect | 382 | 32 | 1973–1986 | 801–2232 | [11] |
| Zhongshan–Dome A | Transect | 583 | 40 | 1994–2011 | 1031–4081 | [12,13] |
| Mawson–Lambert Glacier | Transect | 515 | 36 | 1990–1995 | 1883–2924 | [14] |
| Syowa–Dome F | Transect | 507 | 38 | 1955–2010 | 584–3803 | [15] |
| Princ. Elisabeth | Transect | 58 | 6 | 2009–2012 | 47–1071 | [16] |
| Dronning Maud Land | Scattered | 376 | 104 | 1955–2008 | 1753–3741 | [17,18,19,20] |

[1] Medley et al. (2014), [2] Clausen et al. (1979), [3] Venteris and Whillans (1998), [4] Vaughan et al. (1999), [5] Magand et al. (2007), [6] Frezzotti et al. (2004), [7] Frezzotti et al. (2007), [8] Pettré et al. (1986), [9] Agosta et al. (2012), [10] Verfaillie et al. (2012), [11] Goodwin (1988), [12] Ding et al. (2011), [13] Wang et al. (2016), [14] Higham and Craven (1997), [15] Wang et al. (2015), [16] GLACIOCLIM-BELARE, [17] Picciotto et al. (1968), [18] Mosley-Thompson et al. (1995), [19] Mosley-Thompson et al. (1999), [20] Anschütz et al. (2011).

elevation difference with the observation greater than 200 m (missing elevation of observation is set to Bedmap2 elevation at 1 km resolution). Finally, we bi-linearly interpolate model values of the remaining grid cells at the observation location (see schematic in Fig. S2).

As we restrict our modelling study to the 1979-2015 period, we only consider observations beginning after 1950. For obser-
5    vations beginning after 1979, we time-average model outputs for the same period as the observation. ~~For~~ We keep observations beginning before 1979 ~~, we only consider those covering~~ only if they cover more than eight years, and ~~we time-average model outputs over the full simulated~~ in this case we compare the observed value with the modelled value time-averaged for 1979-2015 ~~period~~.

In a last step, we average-out the kilometre-scale variability of the observed SMB (Agosta et al., 2012) by binning point
10    values onto grid cells. For each grid cell containing multiple observations, we average all observations contained into the grid cell weighted by the time span of observations, and in the same way we weight-average the modelled values interpolated to observation locations. This way, we obtain consistent observed and modelled averaged values on grid cells.

We discard 66 observations beginning before 1979 and spanning less than eight years. We also discard 12 observations for which the four surrounding grid cells fall in ocean, and seven observations located at specific topographic features for which
15    none of the four surrounding grid cell has an elevation difference less than 200 m with respect to the actual location. After this, we retain 559 model-observation comparisons.
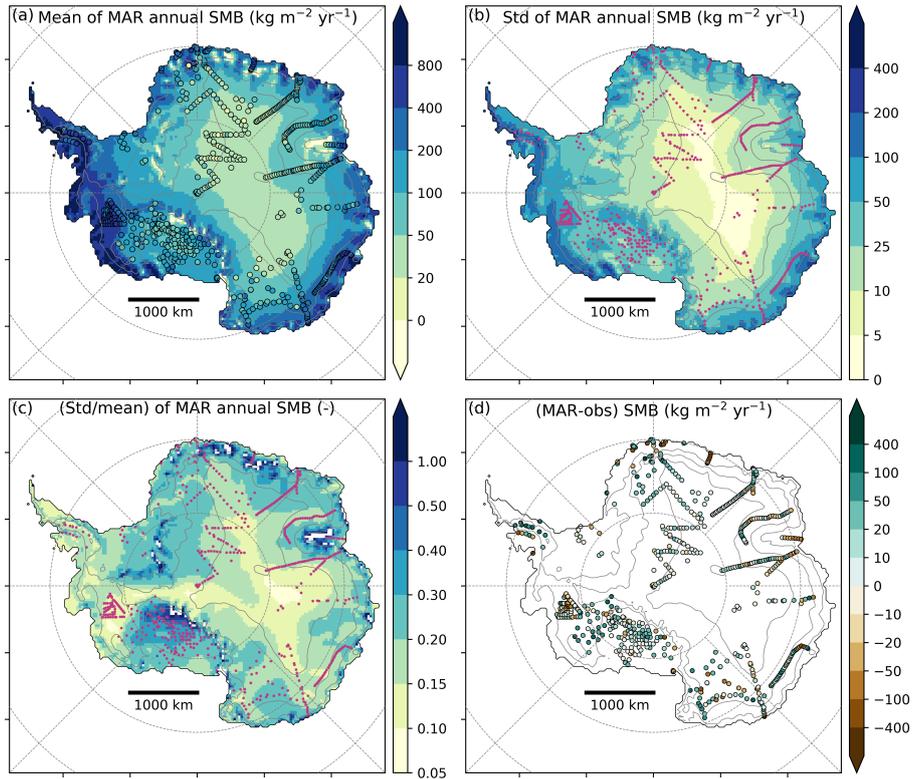
**Figure 1.** MAR SMB for the period 1979-2015: (a) mean annual SMB, with coloured dots showing the observed SMB values (shared colour scale); (b) standard deviation of annual SMB; (c) standard deviation divided by mean annual SMB; (d) difference between MAR and observed SMB on MAR grid cells, following the methodology detailed in Section 2.2.2. Magenta dots in panels b) and c) show the location of SMB observations. Solid grey lines are contours of surface height every 1000 m. Latitude circles are -60°S, -70°S and -80°S, and longitude lines are from 145°W to 145°E by step of 45°.

## 3 Results

### 3.1 Evaluation of the modelled SMB

The large spatial Antarctic SMB gradients, shown in Fig. 1a as modelled by MAR forced by ERA-Interim for the period 1979-2015, coincide with a strong interannual variability (Fig. 1b), expressed by a standard deviation of ∼22% of the mean SMB on average over the ice sheet (Fig. 1c). MAR SMB ~~oscillates around the 559 observed values~~ shows no systematic spatial bias (Fig. 1d), with a mean bias of ~~9~~ 6 kg m$^{-2}$ yr$^{-1}$ (~~7~~4% of the mean observed SMB) ~~and a RMSE of 76~~, as well as a very strong correlation with the observed SMB (R$^2$=0.83, p-value<0.01, computed on the logarithm of SMB values, as SMB distributions are log-normal). RACMO2 shows similar performance (mean bias of -3 kg m$^{-2}$ yr$^{-1}$ ~~(60% of the mean observed SMB~~, R$^2$=0.86, computed on the logarithm of SMB as well).
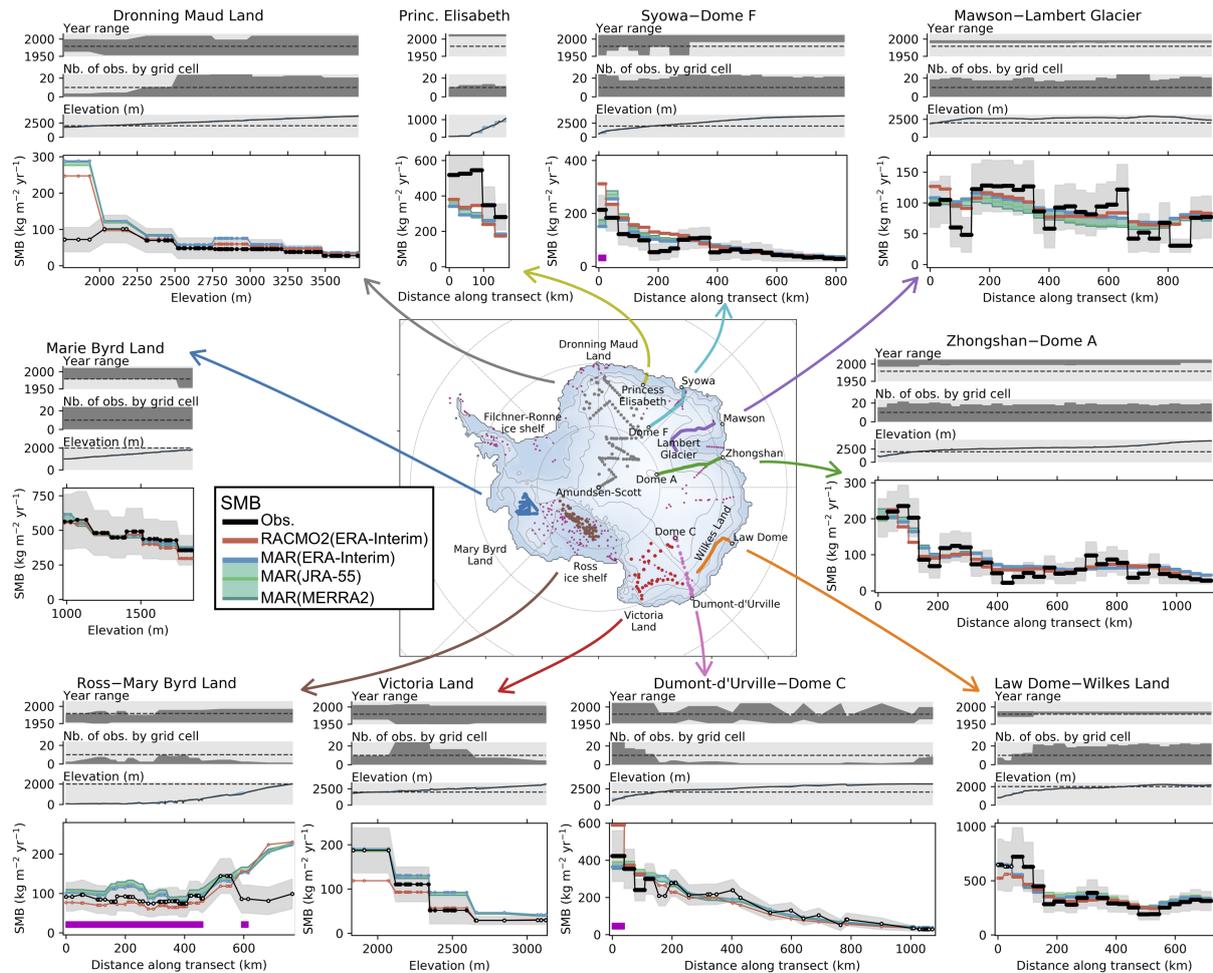
**Figure 2.** Modelled vs. observed SMB for sectors and transects as detailed in Table 1. RACMO2 outputs are bi-linearly interpolated to the MAR grid. SMB values are first averaged on MAR grid cells (Sec. 2.2.2) then along chosen grid direction (Fig. S2) or by elevation bins. Distance along transect starts at the coast. Uncertainty of observed SMB (grey shaded area) is the standard deviation of observations contained in each grid cell (sub-grid variability), estimated as a function of the mean observed SMB (see Fig. S3). Despite SMB values corresponding to grid cell averages, we display one marker for each observation, with the *x* axis corresponding to the observation location along transect or elevation. Markers with white faces are for bins containing less than 10 observations and black faces for bins containing more than 10 observations. Magenta bands mark grid cells where more than 15 % of precipitation sublimates in the katabatic layers according to Grazioli et al. (2017).

The model-observation comparison by sectors (Fig. 2) reveals a good representation of the coast-to-plateau SMB gradients by both RCMs. MAR and RACMO2 are in good agreement despite MAR not including drifting snow processes whereas RACMO2 does, except in Ross–Mary Byrd Land and in Victoria Land where MAR simulates larger SMB than RACMO2.

Another noticeable result is that MAR forced by ERA-Interim, JRA-55 and MERRA2 give very similar results, not only at the observation locations (Fig. 2) but also at the ice sheet scale (Fig. S4, note the colour map scales compared to Fig. S9). This is why we focus on MAR forced by ERA-Interim in the following.

We find no significant differences in the SMB simulated by MAR and RACMO2 when integrated over the ice sheet or its major basins (Table 2). SMB is driven by snowfall amounts, which are more than 10 times larger than other SMB components. Snow sublimation in RACMO2 is the sum of sublimation at the surface of the snowpack and of drifting snow sublimation, and is approximately 50 % larger than in MAR which only includes surface snow sublimation. However, surface snow sublimation alone is almost two times larger in MAR than in RACMO2 (Table 2, also shown in Fig. S5), which we investigate in the next section. Modelled surface melt is less than half of the sublimation amount, however liquid water almost entirely refreezes into the snowpack in both models (maps of modelled melt amounts are shown in Fig. S6). Temporal variability of the SMB and its components is fully driven in both RCMs by the forcing reanalyses and are therefore strongly correlated with each other (time series shown in Fig. S7). We do not elaborate on the SMB temporal variability here as this aspect will be further detailed in a forthcoming study.

## 3.2 ~~Erosion-deposition~~ Drifting snow transport features

~~Oscillations of~~ Fluctuations of the observed SMB around the smooth modelled SMB ~~gradient are particularly~~ gradients are apparent along the four stake transects covering more than 500 km: Law Dome–Wilkes Land, Zhongshan–Dome A, Mawson–Lambert Glacier, and Syowa–Dome F. ~~As snow is usually eroded from topographic crests and collected in valleys, we computed the surface elevation mean curvature to locate crests (positive curvature, convex surface) and valleys (negative curvature, concave surface) in the~~ We related these fluctuations to drifting snow transport. Indeed, the snow eroded from the snowpack is loaded into the atmosphere, where it can sublimate and be transported by the wind. Katabatic winds blowing on the surface of the ice sheet result from the downslope gravity flow of cold, dense air. As a consequence, the surface wind divergence, which drives the snowdrift mass transport, is strongly related to the curvature of the topography (see Fig. S8): slopes becoming steeper (crests, positive curvature) will lead to wind speed acceleration (positive wind divergence), thus to drifting snow export (mass loss), whereas slopes becoming more gentle (valleys, negative curvature) will lead to wind speed deceleration (negative wind divergence), thus to drifting snow deposit (mass gain).

To test our hypothesis, we computed the mean curvature of the MAR $35\times35$ km elevation ~~grid~~field. In Fig. 3, we notice that both RCMs commonly exhibit an excess of accumulation on crests and a deficit of accumulation in valleys, in the range of $\pm40$ kg m$^{-2}$ yr$^{-1}$. To quantify this curvature effect, we correlate MAR SMB bias ($\Delta$SMB) with the curvature. ~~Curvature is shifted by~~ For each transect, we apply a constant shift of $\pm$ one grid cell ~~(2 grid cells for Syowa–Dome F) along each transect according to the~~ to the curvature in order to find the maximum correlation with $\Delta$SMB (Fig. ~~S8).~~ S9). The sign and the amplitude of these shifts are in line with curvature being used as a proxy for wind divergence, as they are consistent with the Coriolis wind deflection westward of the topography gradient (detailed in Fig. S10). When the mean annual 10 m wind speed ($ws_{10}$) is greater than seven m s$^{-1}$, the difference between modelled and observed SMB (in kg m$^{-2}$ yr$^{-1}$) is scaled to approximately $3700\pm1100$ (in $10^6$ kg m$^{-1}$ yr$^{-1}$) times the curvature (in $10^{-6}$ m$^{-1}$), with a significant relationship ($R^2$ =

**9**

**Table 2.** Antarctic integrated SMB on average for 1979-2015 $\pm$ one standard deviation of annual values, in Gt yr$^{-1}$. Antarctic Ice sheet (AIS) and basins geometry are based on Rignot basins (Shepherd et al., 2018). RACMO2 is bi-linearly interpolated on MAR grid and the same mask is applied to both models, with area given for this mask. SMB is computed as follows: MAR SMB = Snowfall + Rainfall − Surface snow sublimation − Run-off; RACMO2 SMB = Snowfall + Rainfall - Surface snow sublimation - Drifting snow sublimation - Drifting snow transport - Run-off.

| Basin | Area ($10^6$ km$^2$) | Component (Gt yr$^{-1}$) | MAR(ERA-Interim) | RACMO2(ERA-Interim) |
|---|---|---|---|---|
| Total AIS w/o Peninsula | 13.41 | SMB | $2200 \pm 115$ | $2177 \pm 107$ |
| | | Snowfall | $2306 \pm 111$ | $2339 \pm 107$ |
| | | Rainfall | $6 \pm 1$ | $2 \pm 1$ |
| | | Surface snow sublimation | $111 \pm 10$ | $57 \pm 4$ |
| | | Drifting snow sublimation | – | $101 \pm 5$ |
| | | Drifting snow transport | – | $5 \pm 0$ |
| | | Run-off | $1 \pm 1$ | $1 \pm 1$ |
| | | Melt | $40 \pm 20$ | $68 \pm 30$ |
| Total AIS | 13.83 | SMB | $2517 \pm 111$ | $2516 \pm 105$ |
| Grounded AIS w/o Peninsula | 12.04 | SMB | $1923 \pm 100$ | $1857 \pm 94$ |
| | | Snowfall | $1995 \pm 97$ | $1987 \pm 94$ |
| | | Surface snow sublimation | $77 \pm 8$ | $39 \pm 3$ |
| | | Drifting snow sublimation | – | $87 \pm 4$ |
| Grounded AIS | 12.27 | SMB | $2120 \pm 99$ | $2068 \pm 93$ |
| Grounded East AIS | 9.77 | SMB | $1170 \pm 89$ | $1121 \pm 80$ |
| | | Snowfall | $1245 \pm 87$ | $1225 \pm 82$ |
| | | Surface snow sublimation | $77 \pm 6$ | $34 \pm 3$ |
| | | Drifting snow sublimation | – | $66 \pm 4$ |
| Grounded West AIS | 2.11 | SMB | $675 \pm 62$ | $643 \pm 62$ |
| | | Snowfall | $675 \pm 61$ | $668 \pm 62$ |
| | | Surface snow sublimation | $1 \pm 3$ | $4 \pm 1$ |
| | | Drifting snow sublimation | – | $20 \pm 2$ |
| Grounded Islands | 0.16 | SMB | $78 \pm 7$ | $93 \pm 8$ |
| Grounded Peninsula | 0.23 | SMB | $198 \pm 26$ | $211 \pm 27$ |

0.430.41, Fig. 4a). For lower wind speed ($ws_{10} < 7$ m s$^{-1}$), we no longer observe any relationship between model bias in SMB
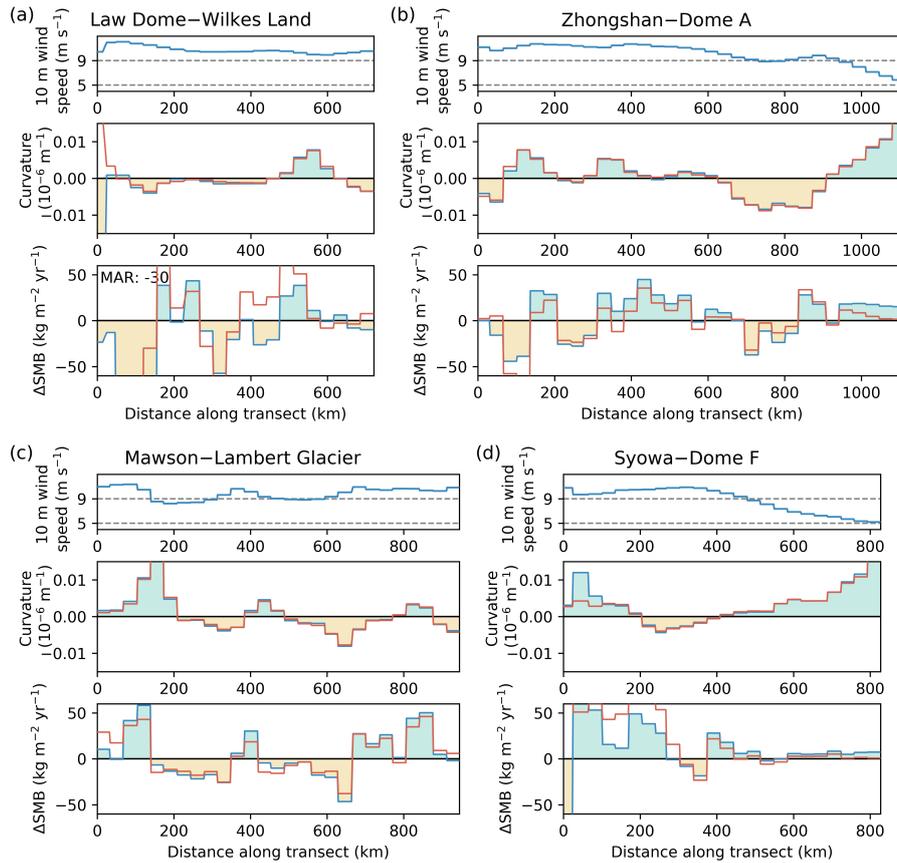
**Figure 3.** For each transect, we show (top) annual mean 10 m wind speed, (middle) curvature of elevation and (bottom) difference in SMB between models and observation. Blue lines and colour shading are for MAR(ERA-Interim) outputs and red lines are for RACMO2(ERA-Interim) outputs. Values are computed as in Fig. 2. For Law Dome–Wilkes Land, MAR SMB is shifted by $-30$ kg m$^{-2}$ yr$^{-1}$.

and curvature (horizontally aligned squares in Fig. 4a). This is consistent with the ~~erosion deposition~~ drifting snow transport process which requires the wind speed to reach threshold values for the erosion to be initiated (Amory et al., 2015).

Hence, a large part of the discrepancies between modelled and observed SMB is explained by elevation curvature when wind speed is sufficiently high, which we relate to the unresolved ~~erosion-deposition process~~ drifting snow transport in MAR. ~~Indeed, katabatic winds blowing on the surface of the ice sheet result from the downslope gravity flow of cold, dense air . As a consequence, surface wind speed is related to the slope of the ice sheet: slopes becoming steeper (positive curvature) will lead to wind speed acceleration, thus to mass export, whereas slopes becoming more gentle (negative curvature)will lead to wind speed deceleration, thus to mass deposit~~We are able to catch the drifting snow transport signal because drifting snow sublimation is negligible for the four studied transects, as they are located at high elevation (>2000 m above sea level – asl), where the cold atmosphere has low capacity to be loaded with moisture (see detailed analysis in Fig. S11). The moisture holding capacity of the atmospheric boundary layer quickly tends to zero when the mean air temperature decreases below

**11**
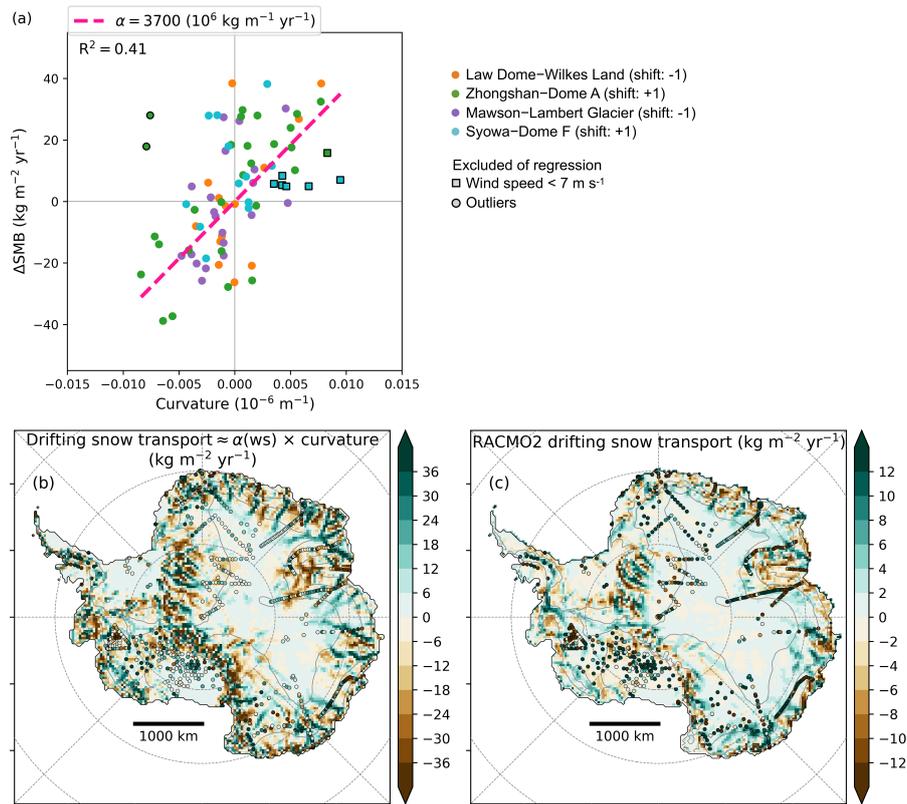
**Figure 4.** (a) Difference in SMB by grid cell (ΔSMB) between MAR(ERA-Interim) and observations for four transects (Law Dome–Wilkes Land, Zhongshan–Dome A, Mawson–Lambert Glacier, and Syowa–Dome F) vs. elevation curvature on MAR grid. Curvature is shifted by ± ~~1-2~~ 1 grid ~~cells~~ cell according to the maximum correlation with ΔSMB (Fig. S8). Linear regression through the origin is plotted with a dashed pink line. We excluded of regression two outliers (dots with black contour) and seven data for which MAR annual 10 m wind speed is lower than 7 m s$^{-1}$ (squares with black contour). (b) Estimate of mean annual ~~erosion-deposition~~ drifting snow transport based on a scaling of the curvature: ~~erosion-deposition~~ drifting snow transport (kg m$^{-2}$ yr$^{-1}$) = $\alpha$ ($10^6$ kg m$^{-1}$ yr$^{-1}$) × curvature ($10^{-6}$ m$^{-1}$), with $\alpha = 0$ kg m$^{-1}$ yr$^{-1}$ for wind speed lower than 5 m s$^{-1}$, $\alpha = 3700$ $10^6$ kg m$^{-1}$ yr$^{-1}$ for wind speed greater than 9 m s$^{-1}$, and $\alpha$ linearly increasing as a function of wind speed in between. Wind speed is the annual mean of 10 m wind speed modelled by MAR(ERA-Interim). Coloured dots show the difference between MAR SMB and observed SMB with the same colour scale. (c) Mean annual ~~erosion-deposition~~ drifting snow transport flux in RACMO2 on average for 1979-2015 (kg m$^{-2}$ yr$^{-1}$). Coloured dots show the difference between MAR SMB and observed SMB with the same colour scale.

-30°C, which is the case along most of the transects, whereas the amplitude of observed SMB fluctuations around the smooth SMB gradient is independent of the temperature (Fig. S12).

In Figure 4b, we propose a spatial estimate of the ~~erosion-deposition~~ drifting snow transport fluxes not resolved by MAR, computed as a simple function of curvature and wind speed as described above. This estimate ~~turns out to be remarkably~~ 5 is comparable to the ~~erosion-deposition~~ drifting snow transport pattern modelled by RACMO2 (Fig. 4c), except that it gives

fluxes approximately three times larger than in RACMO2 (see differences in colour map scales between Fig. 4b and 4c, fluxes summed over the ice sheet and associated uncertainties are detailed in Table S2).

~~The erosion-deposition~~ The drifting snow transport estimate consists in a redistribution of mass with negligible net mass loss over the Antarctic ice sheet (total AIS ~~erosion~~ mass gain of ∼~~80~~ 75 Gt yr$^{-1}$ and total AIS ~~deposition~~ mass loss of ∼~~75~~ 80

5  Gt yr$^{-1}$, see Table S2). ~~It can be interpreted as the transport of suspended snow particles after sublimation in the atmospheric boundary layer, similarly to how erosion-deposition is modelled in RACMO2. Missing~~

Drifting snow sublimation might be the largest mass sink in Antarctica, much larger than the drifting snow transport fluxes at the scale of the ice-sheet (Palm et al., 2017; Lenaerts et al., 2012a). However, we cannot constrain this flux with the available SMB observation dataset, as it occurs bellow 2000 m asl (Fig. S11d), where observations are extremely scarce. Our drifting

10  snow transport estimate can be used to constrain the drifting snow fluxes in models above 2000 m asl, which might have in turn implication for the drifting snow sublimation ~~in MAR is generally compensated by stronger~~ amounts simulated at the ice-sheet margins.

Drifting snow sublimation included in RACMO2 and not in MAR moisten the surface atmospheric layers, consequently reducing the sublimation at the surface of the snowpack. This might explains the stronger surface snow sublimation in MAR

15  than in RACMO2 (Table 2 and Fig. S5)~~, mainly because of dryer atmospheric layers in MAR~~. However, drifting snow sublimation is a potentially larger mass sink than surface snow sublimation, as drifting snow particles are continuously ventilated and fully exposed to the ambient air~~, even though this process is bounded by the water vapour holding capacity of the atmosphere (Bintanja, 2001)~~. Consequently, by accounting for drifting snow in MAR we expect that the drifting snow sublimation mass sink could be enhanced at the expense of surface snow sublimation ~~, at least in areas where surface wind speed is high and the~~

20  ~~atmospheric boundary layer is strongly undersaturated~~ at the ice sheet margins.

## 3.3   Sublimation of precipitation in ~~katabatic channels~~ low-level atmosphere

As described above, the dynamical downscaling of ERA-Interim with RACMO2 and MAR results in similar spatial patterns for SMB as compared to observations. However, at the ice sheet scale, MAR and RACMO2 SMB show regional discrepancies (~~Figure~~Fig. 5a for 2015, similar than the 1979-2015 mean, shown in Fig. S13a) which are primarily the result of differences in

25  simulated snowfall rates (Fig. ~~S9). In this section we focus on areas where RACMO2 snowfall is greater than MAR snowfall by more than 15 %. Those areas are generally located on the east side of valleys (curvatures < -0.005,~~ 5b, and  S13b). We notice that areas where MAR snowfall is much lower than RACMO2 snowfall (Fig. 5~~c) . We relate this to the recent work of Grazioli et al. (2017) which demonstrates that precipitation sublimates in katabatic channels at the ice sheet margins. This is because~~ b, dashed blue lines) coincide almost exactly with the pattern of precipitation that is able to sublimate in the

30  low-level atmosphere according to Grazioli et al. (2017). In this study, the amount of atmospheric sublimation is quantified for the year 2015 using atmospheric modelling constrained with precipitation radar observations. Atmospheric sublimation happens because the katabatic surface air flux, moving from high-elevated inland plateau toward sea level, is subject to adiabatic compression when it moves downslope. This compression induces an increase in air temperature which reduces relative humidity and drives sublimation rates ~~. We find that areas of low-level sublimation derived from observations and modelling~~
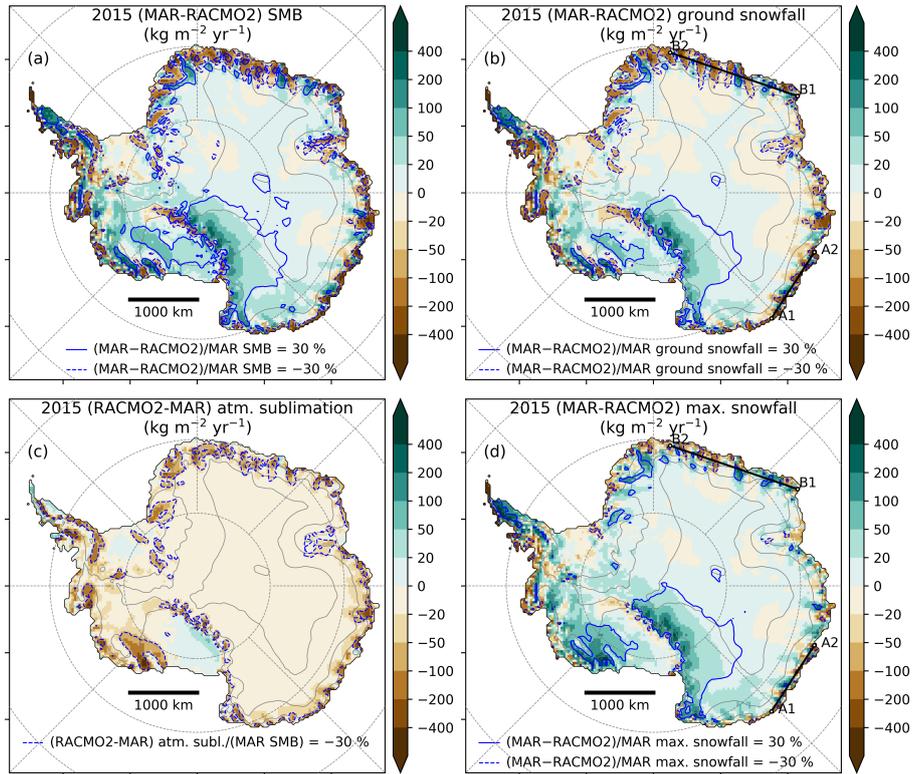
**Figure 5.** The four maps show mass fluxes in $kg\ m^{-2}\ yr^{-1}$ ~~on average~~ for the ~~period 1979-2015.~~ year 2015. (a) Difference in SMB between MAR and RACMO2. ~~Solid blue~~ Blue lines delimitate areas where ~~MAR snowfall~~ the SMB difference is ~~greater than RACMO2 snowfall by more than 15~~ 30 % ~~and solid pink lines areas where RACMO2 snowfall is~~ greater than MAR ~~snowfall by more than 15 %. (b) Difference in snowfall between MAR and RACMO2~~ SMB, with solid lines when MAR ~~snowfall~~ is greater than RACMO2 ~~snowfall by more than 15 %. Pink shading shows areas where curvature is greater than 0.005 (crests). (c) Difference in snowfall between RACMO2~~ and ~~MAR~~ dashed lines when ~~RACMO2 snowfall is greater than~~ MAR ~~snowfall by more than 15 %. Pink shading shows areas where curvature~~ is lower than ~~0.005 (valleys)~~ RACMO2. (~~d~~b) Same as a) but for the snowfall amounts at the ground. (c) Same as a) but ~~with pink shading in areas where~~ for the sublimation of precipitation in the ~~low-level~~ atmospheric layer~~s~~~~is~~. Brown colours and dashed line are for MAR atmospheric sublimation greater than ~~15 % of ground precipitation~~ RACMO2 atmospheric sublimation. (d) Same as ~~estimated by Grazioli et al. (2017)~~ a) but for the ~~year 2015.~~ maximum snowfall amount (equal to ground snowfall plus atmospheric sublimation). Locations of transects A1-A2 and B1-B2 extracted in Fig. 6 are shown in panels b) and d).

~~in Grazioli et al. (2017) coincide almost exactly with areas where MAR snowfall is much lower than~~ in the lower troposphere (∼first 1000 m above the ground), enhanced in the katabatic channels at the ice sheet margins.

To deepen this analysis, we re-ran MAR for the year 2015 in order to save the full atmosphere snowfall fields. From the daily 3D snowfall amounts, we derived the atmospheric sublimation amount from the difference between the maximum snowfall and the ground snowfall in each atmospheric column, as in Grazioli et al. (2017). The same was done for RACMO2~~snowfall~~

(Fig. 5d). In MAR . We find that the atmospheric sublimation simulated by MAR (363 Gt for the year 2015 over the grounded ice sheet) is higher than estimated in Grazioli et al. (2017) (299 Gt after interpolation on the same mask), and much higher than simulated by RACMO2 (128 Gt, Fig 5c). A major difference between MAR and RACMO2 is the advection of precipitation in the atmosphere: in MAR, precipitating particles are explicitly advected through the atmospheric layers until they reach the surface, thus enabled to sublimate in the undersaturated katabatic layers, while in RACMO2, precipitation is added to the surface without advection/sublimation through the atmosphere horizontal advection, and is able to interact with the atmosphere in a single time step only (6 min in this simulation). Consequently, atmospheric sublimation is likely to be underestimated in RACMO2.

We conclude, as in in agreement with Grazioli et al. (2017), that low-level sublimation is an important process atmospheric sublimation is a major mass sink at the ice sheet margins in MAR, as for the period 1979-2015 it may represent ~240±25 of difference in snowfall between RACMO2 and MAR (summed on areas where RACMO2 snowfall is greater than MAR snowfall by more than 15%, Peninsula excluded, ± interannual variability). This value represents 10 year 2015 it represents 16 % of the total MAR snowfall loaded over the ice sheet (Table 2), and 20 snowfall loaded on the grounded ice sheet (12 % in Grazioli et al., 2017), and 26 % for areas under bellow 1000 m above sea level (asl ). We obtain the same quantity for the year 2015, when the amount of snowfall never reaching the ground has been estimated by Grazioli et al. (2017) to be of 240 ± 40 , after interpolation on the MAR grid and for areas where sublimation is greater than ground precipitation by more than 15%, with uncertainty computed by moving this ratio between 10% and 20%. asl (17 % in Grazioli et al., 2017).

It is noticeable that very few SMB observations are available in areas where Grazioli et al. (2017) identify low-level sublimation, marked by magenta bands in Fig. 2. Except for Ross–Mary Byrd Land, the only other areas where low-level sublimation is greater than 15 % of the total precipitation as defined by Grazioli et al. (2017) are close to Dumont d'Urville (coastal Adelie Land) and to Syowa (coastal Dronning Maud Land). In those areas the SMB amount is indeed larger in RACMO2 than in MAR and in observations. Both RCMs overestimate SMB around 2000 m in Dronning Maud Land and in Mary Ross–Mary Byrd Land (Fig. 2), which could indicate katabatic channels not enough resolved by the topography of the models.

### 3.4  SMB overestimation in MAR Precipitation formation and wind glaze areasadvection

MAR simulates significantly larger snowfall amounts than RACMO2 (>15 %) in areas centred on crests under 2000 asl (Fig. 5b, curvature > 0.005). Those locations are the topographic counterparts of katabatic channels outlined in the previous section, where

Differences between MAR and RACMO2 snowfall fields are strongly reduced when considering the maximum snowfall amounts (before sublimation in the low-level atmosphere) rather than the ground snowfall amounts (Fig 5b-d). However, MAR snowfall rates generally exceed those simulated by RACMO2, by more than 30 % on the lee side of the West AIS (Marie Byrd Land toward Ross ice shelf), on the lee side of the Transantarctic Mountains (Victoria Land) and close to crests at the ice sheet margins. MAR maximum snowfall rates are lower than simulated by RACMO2 windward of topographic barriers and in valleys at the ice sheet margins. This spatial pattern looks similar to the one obtained in RACMO2 when delaying the conversion of cloud ice/water into snow/rain (Fig. 3a of van Wessem et al., 2018). This change led to both ice and water
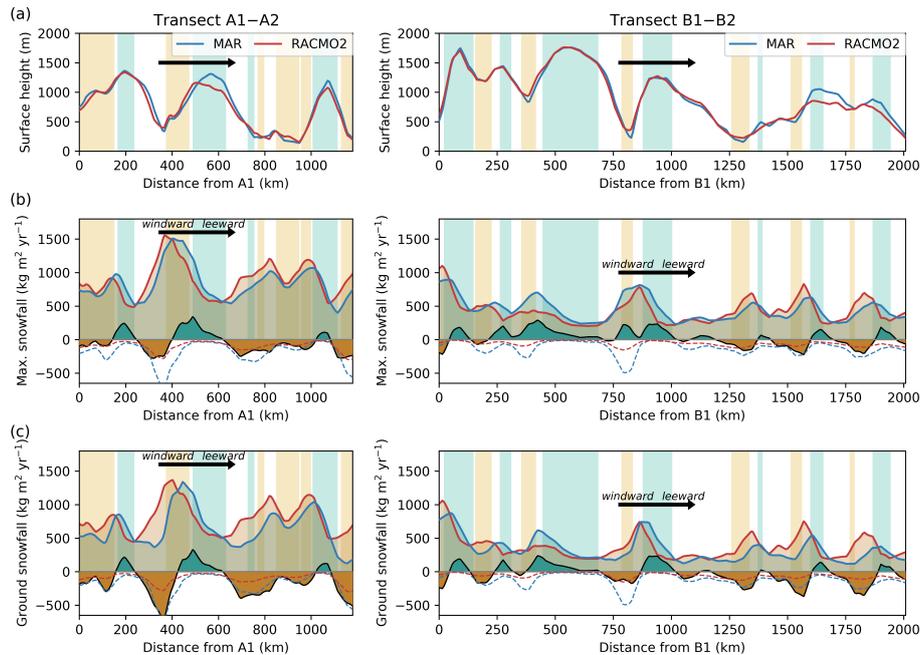
**Figure 6.** MAR and RACMO2 simulated fields for the year 2015, extracted with a bi-linear interpolation for (left) transect A1-A1 and (right) transect B1-B2 (locations shown in Fig. 5b-d). Each panel shows MAR fields (blue lines) and RACMO2 fields (red lines) for (a) surface height, in m asl; (b) maximum snowfall amounts, equal to ground snowfall plus atmospheric sublimation, in $\mathrm{kg\ m^{-2}\ yr^{-1}}$; and (c) snowfall amounts at the ground, in $\mathrm{kg\ m^{-2}\ yr^{-1}}$. In (b) and (c), the thick black line is for the difference in snowfall between MAR and RACMO2 (MAR-RACMO2), with green-filled areas when MAR snowfall is larger than RACMO2 snowfall, and brown-filled areas when MAR snowfall is lower than RACMO2 snowfall (same convention as in Fig. 5); the dotted lines are for the atmospheric sublimation modelled by MAR (blue) and by RACMO2 (red), negative when it induces a decrease in precipitation; light coloured bands show crests (light blue, curvature of MAR topography greater than 0.005) and valleys (light yellow, curvature of MAR topography lower than -0.005). The thick black arrows show the main 800 hPa wind direction during cyclonic activity.

clouds lasting longer in the atmosphere before precipitating and therefore being advected further towards the ice sheet interior (van Wessem et al., 2018).

For a more in-depth analysis, we extract MAR and RACMO2 snowfall ~~is larger than MAR snowfall likely because of missing low-level sublimation of precipitation . MAR also simulates larger snowfall than~~ rates on two transects at the ice sheet margins (Fig. 6), following the main wind direction during cyclonic activities (locations shown in Fig 5b-d). On these transects the observed difference in maximum snowfall between MAR and RACMO2 ~~on the inland plateau.~~is largely explained by a phase difference in the snowfall peaks windward of the topographic barriers, with MAR peaking closer to the crests than RACMO2 (Fig. 6b). This induces a wave-like pattern of precipitation difference strongly related to the shape of the topography, with larger snowfall amounts in MAR than in RACMO2 just windward of crests, and lower snowfall amounts in MAR than

in RACMO2 around windward valleys. At the ground, lower snowfall in MAR than in RACMO2 in valleys is amplified by low-level atmospheric sublimation which peaks in katabatic channels (Fig. 6c).

Observations do not enable to definitively discriminate one model against the other, but we observe a general tendency for MAR to overestimate accumulation on ~~the Ross side of Mary~~ Ross–Mary Byrd Land and close to ice sheet summits (Dome C, Dome A, Dome F, see Fig. 1d and Fig. 2). Close to summits the wind is low, so missing ~~erosion-deposition~~ drifting snow transport process is unlikely explanation for a positive bias in SMB modelled by MAR (Fig. 4~~c~~b). Over the Greenland ice sheet, MAR tends to overestimate ice cores based accumulation inland (Fettweis et al., 2017) while RACMO2 underestimates it (Noël et al., 2018).

~~The larger snowfall amount in MAR than in~~ We conclude that the differences in MAR and RACMO2 ~~is particularly significant south of Victoria Land, on the lee side of~~ snowfall patterns are very likely related to differences in the advection of precipitation inland, which may arise from (i) the different advection of precipitating particles to the ground described in Section 3.3, (ii) different timings of precipitation formation (cloud/precipitation conversion thresholds), and/or (iii) different dynamical response to the ~~Transantarctic Mountains. Simulated snowfall rates in this region are potentially sensitive to cloud microphysics (Fig. 3a of van Wessem et al., 2017), to model resolution via orographic precipitation and foehn effect~~ (topographic forcing, caused either by different dynamical cores or by the different resolutions (the 27 km ~~in~~ resolution in RACMO2 ~~vs~~ better resolves the ice sheet topography than the 35 km ~~in MAR), and to local circulation near the mountains. In this region, we find four grid cells where MAR SMB is significantly larger than observed SMB (Fig. 1d) , which tends to confirm a SMB overestimation in MAR even if those data are composed of point observations possibly not capturing the spatial heterogeneity over 35 grid cell areas. Interestingly, this unobserved area where MAR simulates larger snowfall amounts than RACMO2 is classified as a large wind glaze area in Scambos et al. (2012, see their Fig. 9). In their study, Scambos et al. (2012) outlined that those wind glaze areas could arise from eroded snow sublimating in the undersaturated katabatic layer. This would result in a net mass loss for the ice sheet, as surface snow is moved to suspended snow by the erosion process, then to water vapour by the low-level sublimation process, and subsequently exported outside the ice sheet by the katabatic flow~~resolution in MAR).

## 4   Discussion and conclusion

In our study, we evaluate new estimates of the Antarctic SMB obtained with the polar RCM MAR run for the first time for decades-long simulations at the scale of the whole Antarctic ice sheet. We use model settings comparable to previous MAR simulations over Greenland (Fettweis et al., 2017) but with a specific upper atmosphere relaxation and new ~~fresh~~ surface snow density and roughness length parameterisations. We present the dynamical downscaling of ERA-Interim, JRA-55 and MERRA2 with MAR for the satellite era (1979-2015) where we can rely on reanalyses products. Remarkably, MAR forced by those three reanalyses give similar spatial and temporal SMB patterns. We also compare MAR with the latest simulations of the RCM RACMO2 forced by ERA-Interim ~~(van Wessem et al., 2017)~~(van Wessem et al., 2018). We find no significant differences between MAR and RACMO2 SMB when integrated on the AIS and its major basins (Table 2).

As the dominant feature of the Antarctic SMB is its strong coast to plateau gradient, we extract stake transects and sectors with large elevation ranges from the GLACIOCLIM-SAMBA SMB observational dataset. We show that both RCMs show similar performances when compared to observations, with a good representation of the SMB gradient (Fig. 2). But more importantly, we outline and quantify missing or underestimated processes in both RCMs.

5 Along stake transects, we relate 100 km-scale ~~oscillations~~ fluctuations of observations around the smooth modelled SMB pattern to the shape of the ice sheet captured on the $35 \times 35$ km MAR grid. Both RCMs accumulate too much snow on crests, and not enough snow in valleys, as a result of ~~erosion-deposition processes~~ drifting snow transport fluxes not included in MAR and probably underestimated in RACMO2 by a factor of three (Fig. 4). ~~The~~ In the RACMO2 ~~snowdrift routine separately estimates sublimation of eroded snow and erosion-deposition, the latter being achieved as redistribution of the mass without mass~~
10 ~~change. In MAR, the missing snowdrift sublimation process is compensated by higher sublimation rates at the surface of the snowpack compared to~~ .3p2 version used here, the modified drifting snow routine induced almost halved drifting snow transport and sublimation fluxes compared to the previous RACMO2 ~~(Table 2) driven by dryer surface atmospheric layers in MAR. Widespread wind glaze areas as described in Scambos et al. (2012), formed by the sublimation of eroded snow in the boundary layer, are resolved neither by MAR nor by~~ .3p1 version (Lenaerts and van den Broeke, 2012). In a recent study combining
15 satellite observation of drifting snow events and reanalysis products, Palm et al. (2017) estimate the drifting snow sublimation to be about $\sim$393 Gt yr$^{-1}$ over the Antarctic ice sheet, vs. 181 Gt yr$^{-1}$ in RACMO2 ~~. This is likely because our MAR simulations do not resolve the drifting snow (despite a drifting snow module exists into MAR, e.g. Amory et al., 2015) and~~ .3p1 and 102 Gt yr$^{-1}$ in RACMO2 ~~potentially underestimates drifting snow fluxes~~.3p2 (van Wessem et al., 2018). Consequently, observational constraints from our study and from Palm et al. (2017) both tend to confirm that drifting snow transport and
20 sublimation fluxes are likely much larger than previous model-based estimates and need to be (better) resolved and constrained in climate models.

We also point out that MAR generally simulates larger SMB and snowfall amounts than RACMO2, ~~except in areas where precipitation sublimates while falling through the undersaturated katabatic layer as identified by Grazioli et al. (2017).~~ particularly on the lee side of topographic barriers and on crests at the ice sheet margins. Areas where MAR simulates lower snowfall than
25 RACMO2 are confined windward of topographic barriers and in valleys at the ice sheet margins. We show that this spatial pattern is caused by precipitation being advected further inland in MAR than in RACMO2.

As precipitating snow particles ~~are not advected through the atmospheric layers in~~ have larger time residence in the atmosphere in MAR than in RACMO2 ~~as it is in MAR, the mass difference in areas where MAR snowfall is significantly lower than RACMO2 snowfall can be interpreted as~~ , amounts of precipitation lost by ~~low-level~~ sublimation in katabatic channels ~~. This~~
30 ~~amount represents $\sim$240$\pm$25~~ in MAR are more than twice as much as in RACMO2. Atmospheric sublimation represents 429 Gt yr$^{-1}$ ~~over the ice sheet~~ in MAR over the whole AIS (Peninsula excluded) ~~, which is more than twice the surface snow sublimation (Table 2), 97~~ for the year 2015, 89 % of which is lost below 2000 m asl, and ~~78~~ 61 % below 1000 m asl. This might be of importance for the mass balance of glacier drainage basins ~~(SMB minus discharge, Rignot et al., 2008; Shepherd et al., 2012)~~ (SMB minus discharge, Rignot et al., 2008; Shepherd et al., 2018), as ice streams are typically channel-shaped areas affected
35 by low-level sublimation of precipitation. Consequently, we note the importance of saving precipitation fluxes in models at

least 1300 m above the ground for comparison with CloudSat products, but ideally at all model levels below 1500 m above the ground to be able to compute sublimation of precipitation in the low-level atmospheric layers. This ~~was not the case for MAR and RACMO2 outputs used in this study, but it~~ will become a standard output in forthcoming MAR simulations.

We expect that accounting for drifting snow in MAR will lead to significant improvements in describing the Antarctic SMB and surface climate, as it will enable (1) a quantification of the drifting snow sublimation mass sink, (2) a more realistic representation of relative humidity and temperature in the boundary layer, and (3) an explicit modelling of ~~near-zero accumulation areas (wind glaze areas) and of the redistribution of snow~~ the drifting snow transport from crests to valleys. Exploring the impact of horizontal and vertical model resolution on drifting snow estimates and on sublimation of precipitation in katabatic channels will also be of importance as those processes are related to the shape of the ice sheet and to the advection of precipitation in the atmospheric layers.

traverses in Antarctica and the associated research on climate and surface mass balance modeling, projects ANR-14-CE01-0001 (ASUMA) and ANR-16-CE01-0011 (EAIIST).

# References

Agosta, C., Favier, V., Genthon, C., Gallée, H., Krinner, G., Lenaerts, J. T., and van den Broeke, M. R.: A 40-year accumulation dataset for Adelie Land, Antarctica and its application for model validation, Climate Dynamics, 38, 75–86, 2012.

Amory, C., Trouvillez, A., Gallée, H., Favier, V., Naaim-Bouvet, F., Genthon, C., Agosta, C., Piard, L., and Bellot, H.: Comparison between observed and simulated aeolian snow mass fluxes in Adélie Land, East Antarctica, The Cryosphere, 9, 1373–1383, 2015.

Amory, C., Gallée, H., Naaim-Bouvet, F., Favier, V., Vignon, E., Picard, G., Trouvillez, A., Piard, L., Genthon, C., and Bellot, H.: Seasonal Variations in Drag Coefficient over a Sastrugi-Covered Snowfield in Coastal East Antarctica, Boundary-Layer Meteorology, 164, 107–133, 2017.

Anschütz, H., Sinisalo, A., Isaksson, E., McConnell, J. R., Hamran, S. E., Bisiaux, M. M., Pasteris, D., Neumann, T. A., and Winther, J.-G.: Variation of accumulation rates over the last eight centuries on the East Antarctic Plateau derived from volcanic signals in ice cores, Journal of Geophysical Research: Atmospheres (1984–2012), 116, 456, 2011.

Arthern, R. J., Winebrenner, D. P., and Vaughan, D. G.: Antarctic snow accumulation mapped using polarization of 4.3-cm wavelength microwave emission, Journal of Geophysical Research: Atmospheres (1984–2012), 111, 249, 2006.

Bintanja, R.: Modelling snowdrift sublimation and its effect on the moisture budget of the atmospheric boundary layer, Tellus A: Dynamic Meteorology and Oceanography, 53, 215–232, 2001.

Bromwich, D. H., Fogt, R. L., Hodges, K. I., and Walsh, J. E.: A tropospheric assessment of the ERA-40, NCEP, and JRA-25 global reanalyses in the polar regions, Journal of Geophysical Research: Atmospheres (1984–2012), 112, D10 111, 2007.

Brun, E., David, P., Sudul, M., and Brunot, G.: A numerical model to simulate snow-cover stratigraphy for operational avalanche forecasting, Journal of Glaciology, 38, 13–22, 1992.

Clausen, H. B., Dansgaard, W., Nielsen, J., and Clough, J. W.: Surface accumulation on Ross Ice Shelf, Antarctic Journal of the United States, 14, 68–72, 1979.

De Ridder, K. and Gallée, H.: Land Surface–Induced Regional Climate Change in Southern Israel, Journal of Applied Meteorology, 37, 1470–1485, 1998.

Dee, D. P., Uppala, S. M., Simmons, A. J., Berrisford, P., Poli, P., Kobayashi, S., Andrae, U., Balmaseda, M. A., Balsamo, G., Bauer, P., Bechtold, P., Beljaars, A. C. M., van de Berg, L., Bidlot, J., Bormann, N., Delsol, C., Dragani, R., Fuentes, M., Geer, A. J., Haimberger, L., Healy, S. B., Hersbach, H., Hólm, E. V., Isaksen, L., Kållberg, P., Köhler, M., Matricardi, M., McNally, A. P., Monge Sanz, B. M., Morcrette, J. J., Park, B. K., Peubey, C., de Rosnay, P., Tavolato, C., Thépaut, J. N., and Vitart, F.: The ERA-Interim reanalysis: configuration and performance of the data assimilation system, Quarterly Journal of the Royal Meteorological Society, 137, 553–597, 2011.

Ding, M., Xiao, C., Li, Y., Ren, J., Hou, S., Jin, B., and Sun, B.: Spatial variability of surface mass balance along a traverse route from Zhongshan station to Dome A, Antarctica, Journal of Glaciology, 57, 658–666, 2011.

Eisen, O., Frezzotti, M., Genthon, C., Isaksson, E., Magand, O., van den Broeke, M. R., Dixon, D. A., Ekaykin, A., Holmlund, P., Kameda, T., Karlof, L., Kaspari, S., Lipenkov, V. Y., Oerter, H., Takahashi, S., and Vaughan, D. G.: Ground-based measurements of spatial and temporal variability of snow accumulation in East Antarctica, Reviews of Geophysics, 46, 26 367, 2008.

Ettema, J., van den Broeke, M. R., Meijgaard, E. v., van de Berg, W. J., Box, J. E., and Steffen, K.: Climate of the Greenland ice sheet using a high-resolution climate model – Part 1: Evaluation, The Cryosphere, 4, 511–527, 2010.

Favier, V., Agosta, C., Parouty, S., Durand, G., Delaygue, G., Gallée, H., Drouet, A.-S., Trouvillez, A., and Krinner, G.: An updated and quality controlled surface mass balance dataset for Antarctica, The Cryosphere, 7, 583–597, 2013.

Favier, V., Krinner, G., Amory, C., Gallée, H., Beaumet, J., and Agosta, C.: Antarctica-Regional Climate and Surface Mass Budget, Current Climate Change Reports, 3, 303–315, 2017.

Fettweis, X., Franco, B., Tedesco, M., van Angelen, J. H., Lenaerts, J. T., van den Broeke, M. R., and Gallée, H.: Estimating Greenland ice sheet surface mass balance contribution to future sea level rise using the regional atmospheric climate model MAR, The Cryosphere, 7, 469–489, 2013.

Fettweis, X., Box, J. E., Agosta, C., Amory, C., Kittel, C., Lang, C., van As, D., Machguth, H., and Gallée, H.: Reconstructions of the 1900–2015 Greenland ice sheet surface mass balance using the regional climate MAR model, The Cryosphere, 11, 1015–1033, 2017.

Fretwell, P., Pritchard, H. D., Vaughan, D. G., Bamber, J. L., Barrand, N. E., Bell, R. E., Bianchi, C., Bingham, R. G., Blankenship, D. D., Casassa, G., Catania, G., Callens, D., Conway, H., Cook, A. J., Corr, H. F. J., Damaske, D., Damm, V., Ferraccioli, F., Forsberg, R., Fujita, S., Gim, Y., Gogineni, P., Griggs, J. A., Hindmarsh, R. C. A., Holmlund, P., Holt, J. W., Jacobel, R. W., Jenkins, A., Jokat, W., Jordan, T., King, E. C., Kohler, J., Krabill, W., Riger-Kusk, M., Langley, K. A., Leitchenkov, G., Leuschen, C., Luyendyk, B. P., Matsuoka, K., Mouginot, J., Nitsche, F. O., Nogi, Y., Nost, O. A., Popov, S. V., Rignot, E., Rippin, D. M., Rivera, A., Roberts, J., Ross, N., Siegert, M. J., Smith, A. M., Steinhage, D., Studinger, M., Sun, B., Tinto, B. K., Welch, B. C., Wilson, D., Young, D. A., Xiangbin, C., and Zirizzotti, A.: Bedmap2: improved ice bed, surface and thickness datasets for Antarctica, The Cryosphere, 7, 375–393, 2013.

Frezzotti, M., Pourchet, M., Flora, O., Gandolfi, S., Gay, M., Urbini, S., Vincent, C., Becagli, S., Gragnani, R., Proposito, M., Severi, M., Traversi, R., Udisti, R., and Fily, M.: New estimations of precipitation and surface sublimation in East Antarctica from snow accumulation measurements, Climate Dynamics, 23, 803–813, 2004.

Frezzotti, M., Urbini, S., Proposito, M., Scarchilli, C., and Gandolfi, S.: Spatial and temporal variability of surface mass balance near Talos Dome, East Antarctica, Journal of Geophysical Research: Atmospheres (1984–2012), 112, 195, 2007.

Gallée, H.: Simulation of the Mesocyclonic Activity in the Ross Sea, Antarctica, Monthly Weather Review, 123, 2051–2069, 1995.

Gallée, H. and Gorodetskaya, I. V.: Validation of a limited area model over Dome C, Antarctic Plateau, during winter, Climate Dynamics, 34, 61, 2010.

Gallée, H. and Schayes, G.: Development of a Three-Dimensional Meso-$\gamma$ Primitive Equation Model: Katabatic Winds Simulation in the Area of Terra Nova Bay, Antarctica, Monthly Weather Review, 122, 671–685, 1994.

Gallée, H., Trouvillez, A., Agosta, C., Genthon, C., Favier, V., and Naaim-Bouvet, F.: Transport of snow by the wind: a comparison between Observations in Adélie Land, Antarctica, and Simulations made with the Regional Climate Model MAR, Boundary-Layer Meteorology, 146, 133–147, 2013.

Gallée, H., Preunkert, S., Argentini, S., Frey, M. M., Genthon, C., Jourdain, B., Pietroni, I., Casasanta, G., Barral, H., Vignon, E., Amory, C., and Legrand, M.: Characterization of the boundary layer at Dome C (East Antarctica) during the OPALE summer campaign, Atmospheric Chemistry and Physics, 15, 6225–6236, 2015.

Gardner, A. S., Moholdt, G., Scambos, T. A., Fahnstock, M., Ligtenberg, S., Broeke, M. v. d., and Nilsson, J.: Increased West Antarctic and unchanged East Antarctic ice discharge over the last 7 years, The Cryosphere, 12, 521–547, 2018.

Gelaro, R., McCarty, W., Suarez, M. J., Todling, R., Molod, A., Takacs, L., Randles, C. A., Darmenov, A., Bosilovich, M. G., Reichle, R., Wargan, K., Coy, L., Cullather, R., Draper, C., Akella, S., Buchard, V., Conaty, A., da Silva, A. M., Gu, W., Kim, G.-K., Koster, R., Lucchesi, R., Merkova, D., Nielsen, J. E., Partyka, G., Pawson, S., Putman, W., Rienecker, M., Schubert, S. D., Sienkiewicz, M., and Zhao, B.: The Modern-Era Retrospective Analysis for Research and Applications, Version 2 (MERRA-2), Journal of Climate, 30, 5419–5454, 2017.

Genthon, C., Magand, O., Krinner, G., and Fily, M.: Do climate models underestimate snow accumulation on the Antarctic plateau? A re-evaluation of/from in situ observations in East Wilkes and Victoria Lands, Annals of Glaciology, 50, 61–65, 2009.

Goodwin, I.: Ice sheet topography and surface characteristics in eastern Wilkes Land, East Antarctica, p. 100, ANARE research notes, 1988.

Grazioli, J., Madeleine, J.-B., Gallée, H., Forbes, R. M., Genthon, C., Krinner, G., and Berne, A.: Katabatic winds diminish precipitation contribution to the Antarctic ice mass balance., Proceedings of the National Academy of Sciences of the United States of America, 114, 10 858–10 863, 2017.

Higham, M. and Craven, M.: Surface mass balance and snow surface properties from the Lambert Glacier Basin traverses 1990-94, Tech. rep., 1997.

Kobayashi, S., Ota, Y., Harada, Y., Ebita, A., Moriya, M., Onoda, H., Onogi, K., Kamahori, H., Kobayashi, K., Endo, H., Miyaoka, K., and Takahashi, K.: The JRA-55 Reanalysis: General Specifications and Basic Characteristics, Journal of the Meteorological Society of Japan, 93, 5–48, 2015.

Kuipers Munneke, P., van den Broeke, M. R., Lenaerts, J. T., Flanner, M. G., Gardner, A. S., and van de Berg, W. J.: A new albedo parameterization for use in climate models over the Antarctic ice sheet, Journal of Geophysical Research: Atmospheres (1984–2012), 116, F04 018, 2011.

Lang, C., Fettweis, X., and Erpicum, M.: Future projections of the climate and surface mass balance of Svalbard with the regional climate model MAR, The Cryosphere, 9, 945–956, 2015.

Lenaerts, J. T. and van den Broeke, M. R.: Modeling drifting snow in Antarctica with a regional climate model: 2. Results, Journal of Geophysical Research, 117, D05 109, 2012.

Lenaerts, J. T., van den Broeke, M. R., Déry, S., van Meijgaard, E., van de Berg, W. J., Palm, S. P., and Rodrigo, J.: Modeling drifting snow in Antarctica with a regional climate model: 1. Methods and model evaluation, Journal of Geophysical Research, 117, D05 108, 2012a.

Lenaerts, J. T., van den Broeke, M. R., van de Berg, W. J., van Meijgaard, E., and Munneke, P.: A new, high-resolution surface mass balance map of Antarctica (1979–2010) based on regional atmospheric climate modeling, Geophysical Research Letters, 39, L04 501, 2012b.

Magand, O., Genthon, C., Fily, M., Krinner, G., Picard, G., Frezzotti, M., and Ekaykin, A. A.: An up-to-date quality-controlled surface mass balance data set for the 90°–180°E Antarctica sector and 1950–2005 period, Journal of Geophysical Research, 112, 1, 2007.

Magand, O., Picard, G., Brucker, L., Fily, M., and Genthon, C.: Snow melting bias in microwave mapping of Antarctic snow accumulation, The Cryosphere, 2, 109–115, 2008.

Morcrette, J.-J.: Assessment of the ECMWF Model Cloudiness and Surface Radiation Fields at the ARM SGP Site, Monthly Weather Review, 130, 257–277, 2002.

Mosley-Thompson, E., Thompson, L. G., Paskievitch, J. F., Pourchet, M., Gow, A. J., Davis, M. E., and Kleinman, J.: Recent increase in South Pole snow accumulation, Annals of Glaciology, 21, 131–138, 1995.

Mosley-Thompson, E., Paskievitch, J. F., Gow, A. J., and Thompson, L. G.: Late 20th Century increase in South Pole snow accumulation, Journal of Geophysical Research: Atmospheres (1984–2012), 104, 3877–3886, 1999.

Noël, B., Berg, W. J. v. d., Wessem, J. M. v., Meijgaard, E. v., van As, D., Lenaerts, J. T., Lhermitte, S., Kuipers Munneke, P., Smeets, C. J. P. P., Ulft, L. H. v., Wal, R. S. W. v. d., and van den Broeke, M. R.: Modelling the climate and surface mass balance of polar ice sheets using RACMO2 – Part 1: Greenland (1958–2016), The Cryosphere, 12, 811–831, 2018.

Palm, S. P., Kayetha, V., Yang, Y., and Pauly, R.: Blowing snow sublimation and transport over Antarctica from 11 years of CALIPSO observations, The Cryosphere, 11, 2555–2569, 2017.

Pettré, P., Pinglot, J. F., Pourchet, M., and Reynaud, L.: Accumulation distribution in terre adélie, antarctica: effect of meteorological parameters, Journal of Glaciology, 32, 486–500, 1986.

Picard, G., Brucker, L., Fily, M., Gallée, H., and Krinner, G.: Modeling time series of microwave brightness temperature in Antarctica, Journal of Glaciology, 55, 537–551, 2009.

5   Picciotto, E., Cameron, R., Crozaz, G., Deutsch, S., and Wiloain, S.: Determination of the Rate of Snow Accumulation at the Pole of Relative Inaccessibility, Eastern Antarctica: A Comparison of Glaciological and Isotopic Methods, Journal of Glaciology, 7, 273–287, 1968.

Rignot, E., Bamber, J. L., van den Broeke, M. R., Davis, C., Li, Y., van de Berg, W. J., and van Meijgaard, E.: Rignot, E. et al. Recent Antarctic ice mass loss from radar interferometry and regional climate modelling. Nature Geosci. 1, 106-110, Nature Geoscience, 1, 106–110, 2008.

10   Rignot, E., Velicogna, I., van den Broeke, M. R., Monaghan, A. J., and Lenaerts, J. T.: Acceleration of the contribution of the Greenland and Antarctic ice sheets to sea level rise, Geophysical Research Letters, 38, L05 503, 2011.

Scambos, T. A., Frezzotti, M., Haran, T., Bohlander, J., Lenaerts, J. T., van den Broeke, M. R., Jezek, K., Long, D., Urbini, S., Farness, K., Neumann, T., Albert, M., and Winther, J.-G.: Extent of low-accumulation 'wind glaze' areas on the East Antarctic plateau: implications for continental ice mass balance, Journal of Glaciology, 58, 633–647, 2012.

15   Shepherd, A., Ivins, E. R., Geruo, A., Barletta, V. R., Bentley, M. J., Bettadpur, S., Briggs, K. H., Bromwich, D. H., Forsberg, R., Galin, N., Horwath, M., Jacobs, S., Joughin, I., King, M. A., Lenaerts, J. T., Li, J., Ligtenberg, S. R. M., Luckman, A., Luthcke, S. B., McMillan, M., Meister, R., Milne, G., Mouginot, J., Muir, A., Nicolas, J. P., Paden, J., Payne, A. J., Pritchard, H. D., Rignot, E., Rott, H., Sorensen, L. S., Scambos, T. A., Scheuchl, B., Schrama, E. J. O., Smith, B., Sundal, A. V., van Angelen, J. H., van de Berg, W. J., van den Broeke, M. R., Vaughan, D. G., Velicogna, I., Wahr, J., Whitehouse, P. L., Wingham, D. J., Yi, D., Young, D. A., and Zwally, H. J.: A Reconciled
20   Estimate of Ice-Sheet Mass Balance, Science, 338, 1183–1189, 2012.

Shepherd, A., Ivins, E., Rignot, E., Smith, B., van den Broeke, M. R., Velicogna, I., Whitehouse, P., Briggs, K., Joughin, I., Krinner, G., Nowicki, S., Payne, T., Scambos, T. A., Schlegel, N., A, G., Agosta, C., Ahlstrøm, A., Babonis, G., Barletta, V., Blazquez, A., Bonin, J., Csatho, B., Cullather, R., Felikson, D., Fettweis, X., Forsberg, R., Gallée, H., Gardner, A., Gilbert, L., Groh, A., Gunter, B., Hanna, E., Harig, C., Helm, V., Horvath, A., Horwath, M., Khan, S., Kjeldsen, K. K., Konrad, H., Langen, P., Lecavalier, B., Loomis, B., Luthcke, S.,
25   McMillan, M., Melini, D., Mernild, S., Mohajerani, Y., Moore, P., Mouginot, J., Moyano, G., Muir, A., Nagler, T., Nield, G., Nilsson, J., Noël, B., Otosaka, I., Pattle, M. E., Peltier, W. R., Pie, N., Rietbroek, R., Rott, H., Sandberg-Sørensen, L., Sasgen, I., Save, H., Scheuchl, B., Schrama, E., Schröder, L., Seo, K.-W., Simonsen, S., Slater, T., Spada, G., Sutterley, T., Talpe, M., Tarasov, L., van de Berg, W. J., van der Wal, W., van Wessem, M., Vishwakarma, B. D., Wiese, D., Wouters, B., and team, T. I.: Mass balance of the Antarctic Ice Sheet from 1992 to 2017, Nature, 558, 219–222, 2018.

30   van de Berg, W. J. and Medley, B.: Brief Communication: Upper air relaxation in RACMO2 significantly improves modelled interannual SMB variability in Antarctica, Actes du 25e colloque de l'Association Internationale de Climatologie, 10, 459–463, 2016.

van de Berg, W. J., van den Broeke, M. R., Reijmer, C., and van Meijgaard, E.: Reassessment of the Antarctic surface mass balance using calibrated output of a regional atmospheric climate model, Journal of Geophysical Research: Atmospheres (1984–2012), 111, 159, 2006.

van Wessem, J. M., Reijmer, C., Morlighem, M., Mouginot, J., Rignot, E., Medley, B., Joughin, I., Wouters, B., Depoorter, M. A., Bamber,
35   J. L., Lenaerts, J. T., De Van Berg, W. J., van den Broeke, M. R., and van Meijgaard, E.: Improved representation of East Antarctic surface mass balance in a regional atmospheric climate model, Journal of Glaciology, 60, 761–770, 2014.

van Wessem, J. M., van de Berg, W. J., Noël, B. P. Y., van Meijgaard, E., Birnbaum, G., Jakobs, C. L., Krüger, K., Lenaerts, J. T., Lhermitte, S., Ligtenberg, S. R. M., Medley, B., Reijmer, C. H., van Tricht, K., Trusel, L. D., van Ulft, L. H., Wouters, B., Wuite, J., and van den

Broeke, M. R.: Modelling the climate and surface mass balance of polar ice sheets using RACMO2, part 2: Antarctica (1979-2016), The Cryosphere Discussions, pp. 1–35, 2017.

van Wessem, J. M., Berg, W. J. v. d., Noël, B. P. Y., Meijgaard, E. v., Amory, C., Birnbaum, G., Jakobs, C. L., Krüger, K., Lenaerts, J. T., Lhermitte, S., Ligtenberg, S. R. M., Medley, B., Reijmer, C. H., Tricht, K. V., Trusel, L. D., Ulft, L. H. v., Wouters, B., Wuite, J., and van den Broeke, M. R.: Modelling the climate and surface mass balance of polar ice sheets using RACMO2 – Part 2: Antarctica (1979–2016), The Cryosphere, 12, 1479–1498, 2018.

Vaughan, D. G., Bamber, J. L., Giovinetto, M., Russell, J., and Cooper, A. P. R.: Reassessment of Net Surface Mass Balance in Antarctica, Journal of Climate, 12, 933–946, 1999.

Venteris, E. R. and Whillans, I. M.: Variability of accumulation rate in the catchments of Ice Streams B, C, D and E, Antarctica, Annals of Glaciology, 27, 227–230, 1998.

Verfaillie, D., Fily, M., Le Meur, E., and Magand, O.: Snow accumulation variability derived from radar and firn core data along a 600 km transect in Adelie Land, East Antarctic plateau, The Cryosphere, 6, 1345–1358, 2012.

Vignon, E., Genthon, C., Barral, H., Amory, C., Picard, G., Gallée, H., Casasanta, G., and Argentini, S.: Momentum- and Heat-Flux Parametrization at Dome C, Antarctica: A Sensitivity Study, Boundary-Layer Meteorology, 162, 341–367, 2016.

Wang, Y., Hou, S., Sun, W., Lenaerts, J. T., van den Broeke, M. R., and van Wessem, J. M.: Recent surface mass balance from Syowa Station to Dome F, East Antarctica: comparison of field observations, atmospheric reanalyses, and a regional atmospheric climate model, Climate Dynamics, pp. 1–15, 2015.

Wang, Y., Ding, M., van Wessem, J. M., Schlosser, E., Altnau, S., van den Broeke, M. R., Lenaerts, J. T., Thomas, E. R., Isaksson, E., Wang, J., and Sun, W.: A Comparison of Antarctic Ice Sheet Surface Mass Balance from Atmospheric Climate Models and In Situ Observations, Journal of Climate, 29, 5317–5337, 2016.